Initial axial stiffness of welded RHS T joints

Marsel Garifullin[1], Maria Bronzova[2,3], Sami Pajunen[1], Kristo Mela[1], Markku Heinisuo[1]

[1] *Tampere University of Technology, Tampere, Finland*
[2] *Peter the Great St.Petersburg Polytechnic University, Saint Petersburg, Russia*
[3] *Technical University of Munich, Munich, Germany*

Abstract

Recently, CIDECT (International Committee for the Development and Study of Tubular Structures) has proposed the component method as a unified approach for the design of many types of connections, including welded tubular joints. Although CIDECT provides clear and simple equations for the resistance of welded tubular joints, the design of initial stiffness remains complicated and includes a number of uncertainties. This paper analyzes the theoretical approach for the initial axial stiffness of rectangular hollow section T joints. The validation against experimental data has shown that the component method considerably overestimates the stiffness of T joints. The paper develops new equations for the stiffness of the components “chord face in bending” and “chord side walls in compression”. The equations are based on simplified mechanical models, employing finite element analyses to calculate the parameters for which analytical solutions are found extremely complicated. In addition, the article numerically investigates the effect of chord axial stresses on the axial stiffness of joints and proposes a corresponding chord stress function.

Keywords

Rectangular hollow section; tubular joint; initial stiffness; axial stiffness; component method

1. Introduction

Welded tubular structures are used in a wide range of trusses and frames. In such structures, rectangular hollow section (RHS) joints combine high strength and simple end preparations. The main properties of tubular joints include their design resistance and stiffness. Generally, in the design of joints, the main attention of engineers and scientists is payed to design resistance, while the stiffness of joints is usually disregarded. However, initial stiffness is known to be essential in the global analysis of frames and trusses, since it affects the distribution of forces between members. In addition, it has been shown [1–3] that initial rotational stiffness plays the key role when considering buckling of tubular truss members.

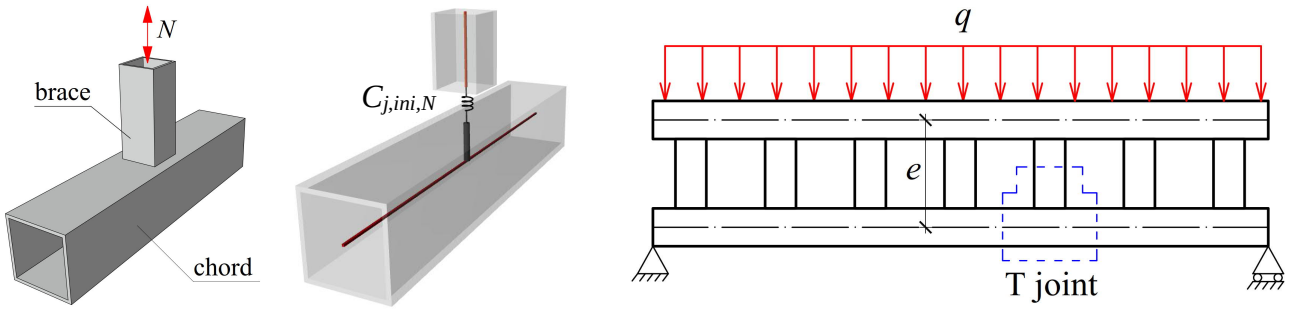

a) b) c)

Fig. 1. a) RHS T joint loaded by axial force; b) axial stiffness modelled by a linear spring; c) Vierendeel girder.

Particular attention should be paid to axial stiffness, which represents the stiffness of a joint under an axial force acting along its brace. Fig. 1a shows an RHS T joint loaded by an axial force. A T joint represents the simplest joint configuration, when a brace is welded to a chord at an angle of 90°. Considering a beam model for such a joint, its axial stiffness $C_{j,ini,N}$ can be presented by a linear spring located on the surface of the chord [4]. The importance of axial stiffness for such joints can be demonstrated in a shallow Vierendeel girder, shown in Fig. 1c. When the girder is analyzed using the frame theory, then in addition to rotational stiffness, the axial stiffness of its joints should be taken into account. The local deformations of the joints can reduce the height of the girder *e*. Such reduction can

be particularly noticeable for shallow girders. Finally, this increases axial forces acting in the chords, making the design unsafe.

The current design rules for RHS T joints in EN 1993-1-8:2005 [5] and CIDECT Design Guide No. 3 [6] are based on the failure mode approach and allow calculating design resistance, providing however no information for initial stiffness. Most of the publications and design guides on the topic [7–9] deal with the resistance of RHS joints, and very few of them investigate their stiffness. A formula for the initial axial stiffness of circular hollow section joints was presented by Mäkeläinen et al. [10]. Grotmann & Sedlacek [11] investigated the initial stiffness of RHS joints under in-plane bending. An extensive parametric study of axially-loaded joints was conducted by de Matos et al. [12], but no theoretical equation was proposed for initial stiffness. Costa-Neves [13] developed the equation for the axial stiffness of RHS-to-IPE connections, which was later accepted by CIDECT [14] and extended for RHS joints with some modifications.

One of the most reliable solutions for the design of initial stiffness can be provided by the component method. It was invented by Zoetemeijer [15] for bolted beam-to-column connections and developed by Tschemmernegg [16]. Later it was extended to column bases by Wald [17] and fire resistance by Leston-Jones [18]. Girão Coelho & Bijlaard [19] employed the method to investigate the behavior of high strength steel end-plate connections. Da Silva [20] developed the component method for joints under arbitrary loading. For bolted end-plate joints the method was used by Heinisuo et al. [21].

Decomposing the joint into basic parts (components), the component method determines joint resistance and stiffness by combining the resistance and stiffness of these components. Being a unified approach for the design of various types of joints, the method was adopted by EN 1993-1-8:2005 [5] for joints connecting H or I sections. Weynand & Jaspart [22] proposed the method for hollow section joints. The main principles of the component method for tubular joints were developed in the CIDECT reports 5BP [23] and 16F [14]. The documents identify the main components of RHS joints and present a detailed procedure to calculate their design resistance. However, the information concerning initial stiffness is very limited: the provided equations for the stiffness of the components are not distinguished between various loading cases, and, therefore, the design of initial stiffness remains questionable.

This paper investigates the theoretical approach for the initial axial stiffness of RHS T joints. Section 2 briefly describes and discusses the current design procedure for axial stiffness, which is provided in the CIDECT report 16F [14] (hereinafter – CIDECT). Section 3 validates the design approach against the experimental data available in the literature. Section 4 develops and experimentally validates new stiffness equations for two individual components. The equations are based on simple mechanical models, employing finite element modeling to replace complicated analytical solutions. Finally, Section 5 numerically investigates the effect of chord axial stresses on the axial stiffness of RHS T joints and develops a corresponding chord stress function. The developed solutions are limited only for joints following the requirements of EN 1993-1-8:2005 [5].

2. Current theoretical approach for the initial axial stiffness of RHS T joints

The main notations of RHS T joints are provided in Fig. 2a. The theoretical approach for the initial stiffness of tubular joints employs the component method, as presented in CIDECT [14]. The component method assumes the axial load to be transferred from the brace to the chord face through four loading zones located at the corners of the brace. The mechanical behavior of the joint can then be modelled by a system of springs, as shown in Fig. 2b. Generally, the springs represent the following components:

a) chord face in bending,
b) chord side walls in tension / compression,
c) chord side walls in shear,
d) chord face under punching shear,
e) brace flange / webs in tension / compression,
f) chord section in distortion,
g) welds.

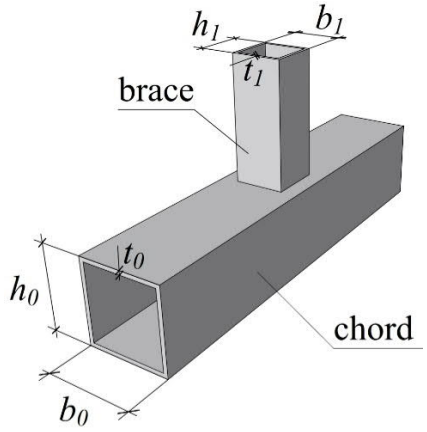

b_0	Chord width
h_0	Chord height
t_0	Chord wall thickness
b_1	Brace width
h_1	Brace height
t_1	Brace wall thickness
β	b_1/b_0 ratio
η	h_1/b_0 ratio
γ	$b_0/2t_0$ ratio
a_w	Weld throat thickness

a)

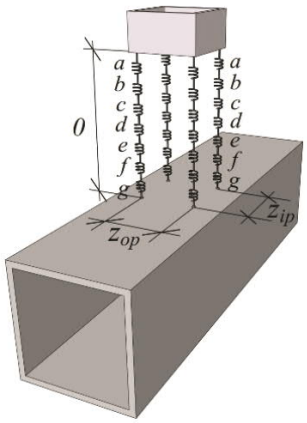

b)

Fig. 2. RHS T joint: a) notations; b) component model.

The behavior of the springs is assumed to be elastic. The initial stiffness of the joint is computed by combining the corresponding stiffnesses of the components using the combination rules for the systems of springs. In particular, initial axial stiffness $C_{j,ini,N}$ is calculated as

$$C_{j,ini,N} = \frac{E}{\sum_i \frac{1}{k_i}}, \tag{1}$$

where E is Young's modulus, and k_i is the stiffness of component i. In this paper, k_i defines the sum of the four components (strings) in the corners of the brace; therefore, each component is counted in Eq. (1) only once. According to [4], only components a "chord face in bending" and b "chord side wall in compression / tension" play a noticeable role in the axial stiffness of RHS T joints. The other components have substantially greater stiffness and can be considered as infinite for practical purposes. Taking into account the aforementioned assumptions, Eq. (1) can be reduced to

$$C_{j,ini,N} = \frac{E}{\frac{1}{k_a} + \frac{1}{k_b}} \tag{2}$$

where k_a is the stiffness of the component "chord face in bending" and k_b is the stiffness of the component "chord side walls in compression / tension". According to CIDECT [14], the stiffness of the latter is assumed to be the same in tension and in compression. This paper considers joints only under compressive axial load; therefore, component b is referred to as "chord side walls in compression" for simplicity. For joints with large β, the stiffness of the component "chord face in bending" becomes relatively high, i.e. $0.1k_a > k_b$, and can be also ignored in the design of initial stiffness. In this case, Eq. (2) can be simplified to

$$C_{j,ini,N} = Ek_b \tag{3}$$

2.1 Component "Chord face in bending"

As been said before, the stiffness of the component "chord face in bending" has to be calculated only for the joints in which this component noticeably contribute to the design of stiffness. To be consistent with the design of resistance specified in EN 1993-1-8:2005 [5], such joints can be limited to those governed by chord face failure, i.e. $\beta \leq 0.85$. However, this component might become irrelevant even for smaller β if the cross-section of the brace is increased by large fillet welds [24].

Two possible options are available to compute the stiffness of this component. The first one was developed by Costa-Neves [13] for RHS-to-IPE connections. Later it was accepted by CIDECT [14] in a form presented in Eq. (4).

$$k_a = \frac{t_0^3}{14.4\beta_0 L_{stiff}^2}\left(\frac{L_{stiff}^2}{bt_0}\right)^{1.25} \cdot \frac{\frac{c}{L_{stiff}} + \left(1-\frac{b}{L_{stiff}}\right)\tan\theta}{\left(1-\frac{b}{L_{stiff}}\right)^3 + \frac{10.4\left(1.5-1.6\frac{b}{L_{stiff}}\right)}{\left(\frac{L_{stiff}}{t_0}\right)^2}} \tag{4}$$

where b and c are respectively the width and the height of the brace, i.e., $b = b_1$ and $c = h_1$. L_{stiff} is the stiffness length determined as $L_{stiff} = d + r$, where d and r represent the width of the chord top face flat area and the chord inner corner radius, respectively. Notations b, c, d and r are illustrated in Fig. 3. The reduction factor β_0 is found as

$$\beta_0 = \begin{cases} 1, & \frac{b+c}{L} \geq 0.5 \\ 0.7 + 0.6\frac{b+c}{L}, & \frac{b+c}{L} < 0.5 \end{cases} \tag{5}$$

$$L = d + 0.5r$$

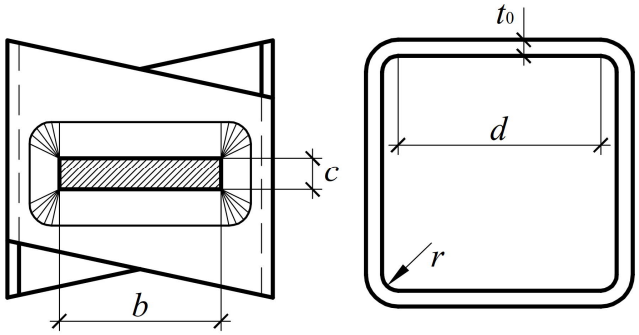

Fig. 3. Design model for component “chord face in bending”.

The angle θ is defined as

$$\theta = \begin{cases} 35 - 10b / L_{stiff}, & b / L_{stiff} < 0.7 \\ 49 - 30b / L_{stiff}, & b / L_{stiff} \geq 0.7 \end{cases} \tag{6}$$

The validity range of Eq. (4) is defined by the following limitations:

$$10 \leq L_{stiff} / t_0 \leq 50; \quad 0.08 \leq b / L_{stiff} \leq 0.75; \quad 0.05 \leq c / L_{stiff} \leq 0.20 \tag{7}$$

For RHS joints, the last limitation in Eq. (7) is transformed into

$$0.05 \leq h_1 / L_{stiff} \approx h_1 / b_0 = \eta \leq 0.20 \tag{8}$$

Obviously, this requirement can be fulfilled only for very small braces, meaning that Eq. (4) violates by default its validity range for most of RHS joints. However, Eq. (4) will be examined in this paper.

The second option for the stiffness of the component “chord face in bending” has been presented in [25] and accepted as an alternative approach in CIDECT [14]. It represents the following equation:

$$k_a = \frac{\pi t_0^3}{12\left(1-\nu^2\right)C_t\left(\frac{b_0 - t_0}{2}\right)^2} \tag{9}$$

where ν is Poisson’s ratio and C_t is a coefficient assumed as 0.18. It should be noted that Eq. (9) represents a function of the chord geometry and does not depend on the size of the brace, making its reliability doubtful for tubular joints. CIDECT [14] provides no information regarding its validity range.

2.2 Component “Chord side walls in compression”

The stiffness of the component “chord side walls in compression” was originally developed in [26] and later studied in [27]. The component employs the model of an RHS chord loaded by two transverse plates of the same width as the chord, as shown in Fig. 4a. CIDECT [14] provides the following equation for its stiffness:

$$k_b = \frac{2 \cdot 0.7 \cdot b_{eff,c,wc} \cdot t_0}{h_0} \tag{10}$$

where $b_{eff,c,wc}$ is the effective width, defined as

$$b_{eff,c,wc} = t_1 + 2\sqrt{2}a_w + 5t_0 \tag{11}$$

where t_1 is the thickness of the loading plate. In case of an RHS joint, the load is transferred through the whole section of the tubular brace, as shown in Fig. 4b, and Eq. (11) should be modified as

$$b_{eff,c,wc} = h_1 + 2\sqrt{2}a_w + 5t_0 \tag{12}$$

However, the applicability of Eq. (10) for tubular joints remains questionable. Firstly, as can be seen in Fig. 4a, Eq. (10) has been developed for X joints and CIDECT [14] does not specify its reliability for T joints. Secondly, Eqs. (10)-(12) do not include β as a variable, i.e., provide the same solution for joints with the same h_1 but various b_1. Since these equations have been developed for β = 1.0, their applicability for joints with smaller β remains unclear.

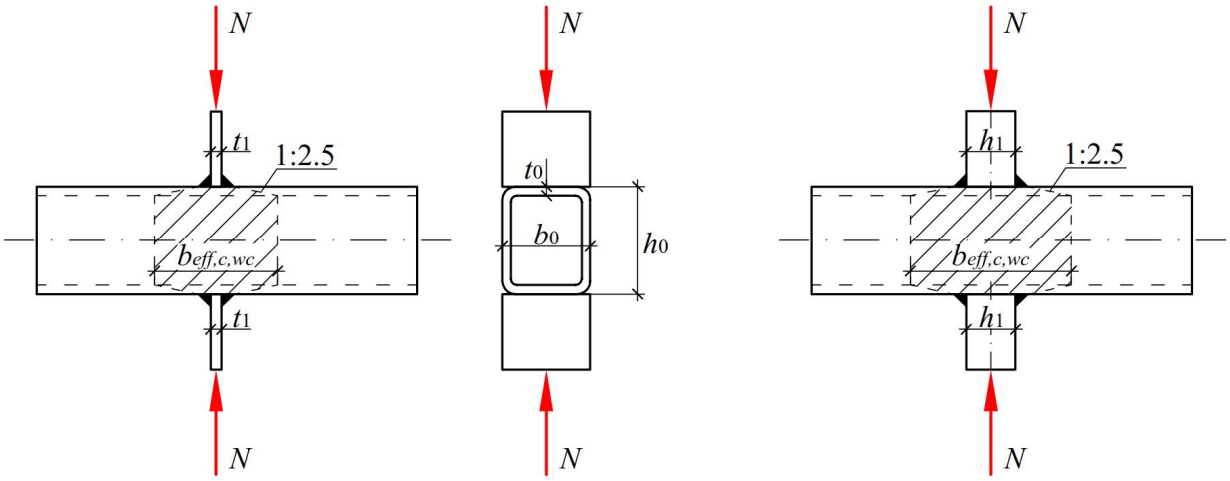

Fig. 4. Component “chord side walls in compression”: a) original design model; b) its extension to RHS joints.

3. Validation of the current theoretical approach

This part validates the current approach for the initial axial stiffness of RHS T joints with the experimental results available in the literature. Usually publications dealing with experimental investigations of joints provide no direct values of initial stiffness. For this reason, initial stiffness was determined graphically, as a tangent line in the beginning of available load-displacement curves. The described procedure is illustrated in Fig. 5, where $C_{j,ini,N}$ denotes initial axial stiffness. Although the accuracy of this approach is doubtful, it represents the only possible method to obtain experimental stiffness from available publications. Moreover, the design of initial stiffness does not require such high level of accuracy as the design of resistance, assuming 30% discrepancy in both directions. This fact can fully justify the possible inaccuracy of this method. For simplicity, initial axial stiffness is denoted as C further in this paper.

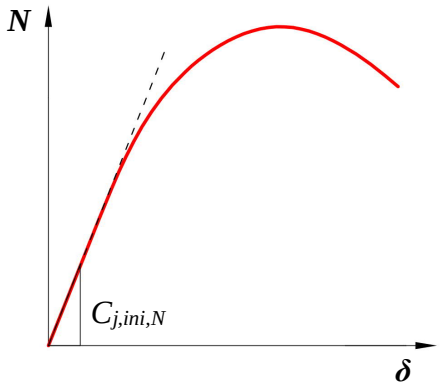

Fig. 5. Graphical approach for determination of initial axial stiffness.

A pioneering experimental work on T joints has been conducted by Kato & Nishiyama [28]. However, the authors presented only the global deformations of joints, including chord bending. Later a series of tests under various loading was conducted by Zhao & Hancock [29], but only three load-displacement curves can be found for T joints under pure axial loading. One T joint was selected from the tests of Davies & Crockett [30]. Nizer et al. [31] conducted six tests on T joints with and without axial loading in the chord. Generally, axial stresses in the chord are found to affect the stiffness of T joints; therefore, only one joint free from chord pre-loading have been selected for the validation. Some results have been found in the most recent tests of Becque & Wilkinson [32].

Attention should be also paid to the publications that analyze the behavior of RHS X joints, e.g. [33, 34]. Due to the similarities in the behavior of T and X joints, these joints are often considered together. In particular, EN 1993-1-8:2005 [5] and CIDECT Design Guide No. 3 [6] provide the same equations for the design resistances of RHS T and X joints. However, the design of initial stiffness might differ. To investigate this issue in details, a comparative analysis was conducted based on the experimental results of Feng & Young, who conducted a series of tests on stainless steel RHS T [35] and X [36] joints. The tests were carried out in such a way that the geometry of X joints repeated the geometry of some T joints. The stiffness of the joints with matching geometry was determined and collected in Table 1, where the joints are arranged in the ascending order of β. The graphical comparison of the behavior of some matching joints is provided in Fig. 6.

Table 1. Comparison of stiffness of T and X joints. The names of joints in accordance with [35] and [36].

X joint	C_X [kN/mm]	T joint	C_T [kN/mm]	C_X/C_T	β
XD-C140x3-B40x2-P0	75	TD-C140x3-B40x2	42	1.8	0.50
XH-C110x4-B150x6-P0	200	TH-C110x4-B150x6	50	4.0	0.75
XD-C50x1.5-B40x2-P0	200	TD-C50x1.5-B40x2	67	3.0	0.80
XD-C40x2-B40x2-P0	1900	TD-C40x2-B40x2	167	11.4	1.00
XD-C50x1.5-B50x1.5-P0	1700	TD-C50x1.5-B50x1.5	100	17.0	1.00
XD-C140x3-B140x3-P0	4250	TD-C140x3-B140x3	175	24.3	1.00
XH-C150x6-B150x6-P0	2000	TH-C150x6-B150x6	338	5.9	1.00
XH-C200x4-B200x4-P0	1500	TH-C200x4-B200x4	145	10.3	1.00
XN-C40x2-B40x2-P0	2000	TN-C40x2-B40x2	100	20.0	1.00

It can be seen that X joints have noticeably higher experimental stiffness than matching T joints. The difference is particularly pronounced for the cases with $\beta = 1.0$, reaching an order of magnitude for some joints. The observed difference can be explained by the various contribution of the components to the overall stiffness of the joint. If β is small, the stiffness is mostly governed by the component “chord face in bending”, which behaves similarly for both types of joints. This leads to relatively small difference between the stiffness of T and X joints. Oppositely, the stiffness of the joints with large β is mostly influenced by the component “chord side walls in compression”, which obviously behaves differently for T and X joints. This leads to a significant difference in the stiffness of the matching T and X joints. These results demonstrate that initial stiffness should be calculated differently for T and X joints. Although a common equation can be adopted for the component “chord face in bending”, individual equations for T and X joints should be derived for the component “chord side walls in compression”. For this reason, X joints are not employed in the validation and this paper considers only T joints.

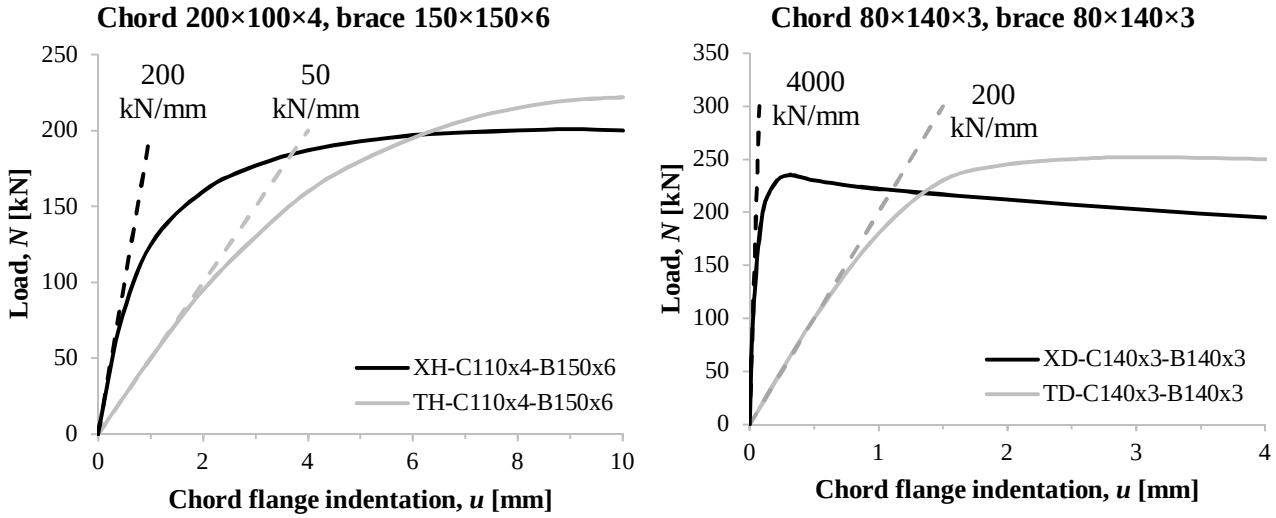

a) b)

Fig. 6. Comparison of T and X joints with matching geometry: a) $\beta = 0.75$, b) $\beta = 1.0$.

Attention should be also paid to stainless steel joints. Due to the non-linear stress-strain responses of stainless steels [34], the equation developed for joints made of carbon steels may be invalid for joints made of stainless steels. For this reason, the latter were excluded from in the validation, in particular the abovementioned tests of Feng & Young [35]. Table 2 presents the summary of the tests used for the validation. Table 3 provides the details of the joints and their experimental initial stiffness C_{exp}, which was determined according to Fig. 5.

Table 2. Summary of tests used for the validation.

No.	Authors	Reference
1-3	Zhao & Hancock, 1991	[29]
4	Nizer et al., 2016	[31]
5-6	Becque & Wilkinson, 2017	[32]
7	Davies & Crockett, 1996	[30]

Table 3. Details of joints used for the validation.

No.	Joint	b_0 [mm]	h_0 [mm]	t_0 [mm]	$r^{1)}$ [mm]	b_1 [mm]	h_1 [mm]	t_1 [mm]	β	2γ	a_w [mm]	$E^{2)}$ [GPa]	C_{exp} [kN/mm]
1	S1B1C11	51	102	4.9	4.9	51	51	4.9	1.00	10.4	4.6	200	570
2	S1B1C12	51	102	3.2	3.2	51	51	4.9	1.00	15.9	4.6	200	330
3	S1B1C23	102	102	4	4	51	51	4.9	0.50	25.5	4.6	200	74
4	TN02N0	140	80	4	4	100	100	3	0.71	35.0	5.0	200	280
5	T1	200	200	6	14	100	100	8	0.50	33.3	4.0	210*	75
6	T4	400	400	16	24	200	200	12.5	0.50	25.0	6.3	210*	400
7	MPJT1	150	150	6.2	9.3	90	90	6.2	0.60	24.2	6.2	210*	230

[1)] nominal inner corner radius;

[2)] Young's modulus of the chord steel (* if a value not provided by authors).

Theoretically, initial stiffness was calculated according to Section 2. For the joints with $\beta \leq 0.85$, the stiffness of the component "chord face in bending" was computed using both available options, Eqs. (4) and (9), corresponding to k_{a1} and k_{a2} respectively. The stiffness of the component "chord side walls in compression" was calculated by Eq. (10). It should be noted that most of the joints were welded with fillet welds, which are known to considerably increase their initial stiffness [37]. In this paper, the influence of fillet welds was taken into account using the approach of de Matos et al. [12], which replaces the actual brace section by the equivalent butt-welded section with the following width:

$$b_{eq} = b_1 + 1.6a_w \tag{13}$$

The equivalent brace width was used further to calculate the equivalent brace-to-chord width ratio:

$$\beta_{eq} = b_{eq} / b_0 \leq 1.0 \tag{14}$$

The equivalent brace-to-chord width ratio was further used to compute the stiffnesses k_a and k_b. Two joint stiffnesses, C_1 and C_2, were calculated according to Eq. (2), respectively employing k_{a1} and k_{a2} for the component "chord face in bending". For the joints with $\beta > 0.85$, only the component "chord side walls in compression" was considered, and joint stiffness C was determined according to Eq. (3).

Table 4 provides a detailed comparison of initial stiffness calculated theoretically and experimentally. Regarding the joints with $\beta \leq 0.85$, if k_a is calculated using the first approach, Eq. (4), then theoretical stiffness two times overestimates the experimental. Oppositely, if k_a is calculated using the alternative approach, Eq. (9), the results are significantly underestimated, with the average C_2 / C_{exp} ratio of 0.08. For the joints with $\beta > 0.85$, the stiffness is overestimated more than two times. All these findings clearly show that the CIDECT equations for the initial stiffness of RHS T joints cannot serve as a reliable tool in the design of tubular joints and more accurate equations have to be developed.

Table 4. Validation of the theoretical approach.

No.	Joint	β	β_{eq}	E [GPa]	k_{a1} [mm]	k_{a2} [mm]	k_b [mm]	C_1 [kN/mm]	C_2 [kN/mm]	C_{exp} [kN/mm]	C_1 / C_{exp}	C_2 / C_{exp}
	$\beta \leq 0.85$											
3	S1B1C23	0.50	0.57	200	0.661	0.043	4.612	116	8.4	74	1.6	0.11
4	TN02N0	0.71	0.77	200	4.064	0.022	9.390	567	4.4	280	2.0	0.02
5	T1	0.50	0.53	210	0.747	0.037	5.935	139	7.7	75	1.9	0.10
6	T4	0.50	0.53	210	2.317	0.178	16.670	427	36.9	400	1.1	0.09
7	MPJT1	0.60	0.67	210	2.883	0.074	8.017	445	15.3	230	1.9	0.07
	Average										**2.0**	**0.08**
	Variance										**0.3**	**0.001**
	$\beta > 0.85$											
1	S1B1C11	1.00	1.00	200	-	-	5.952	1190	-	570	2.1	-
2	S1B1C12	1.00	1.00	200	-	-	3.514	703	-	330	2.1	-
	Average										**2.1**	
	Variance										**0.0**	

4. New equations for the stiffness of components

Given the unsatisfactory prediction of initial axial stiffness by the current theoretical approach, this section develops a more accurate solution for RHS T joints. Following the component method, the paper proposes new equations for the components "chord face in bending" and "chord side walls in compression". To avoid extremely complicated analytical solutions for these components, the paper considers simplified mechanical models and employs the concept of equivalent length and width, which are determined numerically. The developed equations are further validated against the same experimental results.

4.1 Stiffness of the component "chord face in bending"

Consider an RHS T joint with a $b_0 \times h_0 \times t_0$ chord loaded axially by a $b_1 \times h_1$ brace, as shown in Fig. 7a. Generally, the thickness of the brace t_1 does not influence the structural properties of tubular joints [38]; therefore, it is not considered in this section. Since the influence of fillet welds is considered independently (see Section 3), it is ignored in this study. The top face of the chord can be replaced by a simply supported plate with an equivalent length l_{eff} and a span $L = b_0 - 2t_0$. The load N can be assumed applied through an infinitely rigid plate of the size $b_1 \times l_{eff}$. This design model can be simplified further to a 2D beam model, shown in Fig. 7b. The vertical displacement of point A (mid-point of the 2D beam) is found as

$$v(A) = \frac{N(L - b_1)^3}{48EI} \tag{15}$$

where I is the second moment of area of the cross-section A-A. Then, Eq. (15) can be written as

$$v(A) = \frac{N(L - b_1)^3}{4El_{eff}t_0^3} \tag{16}$$

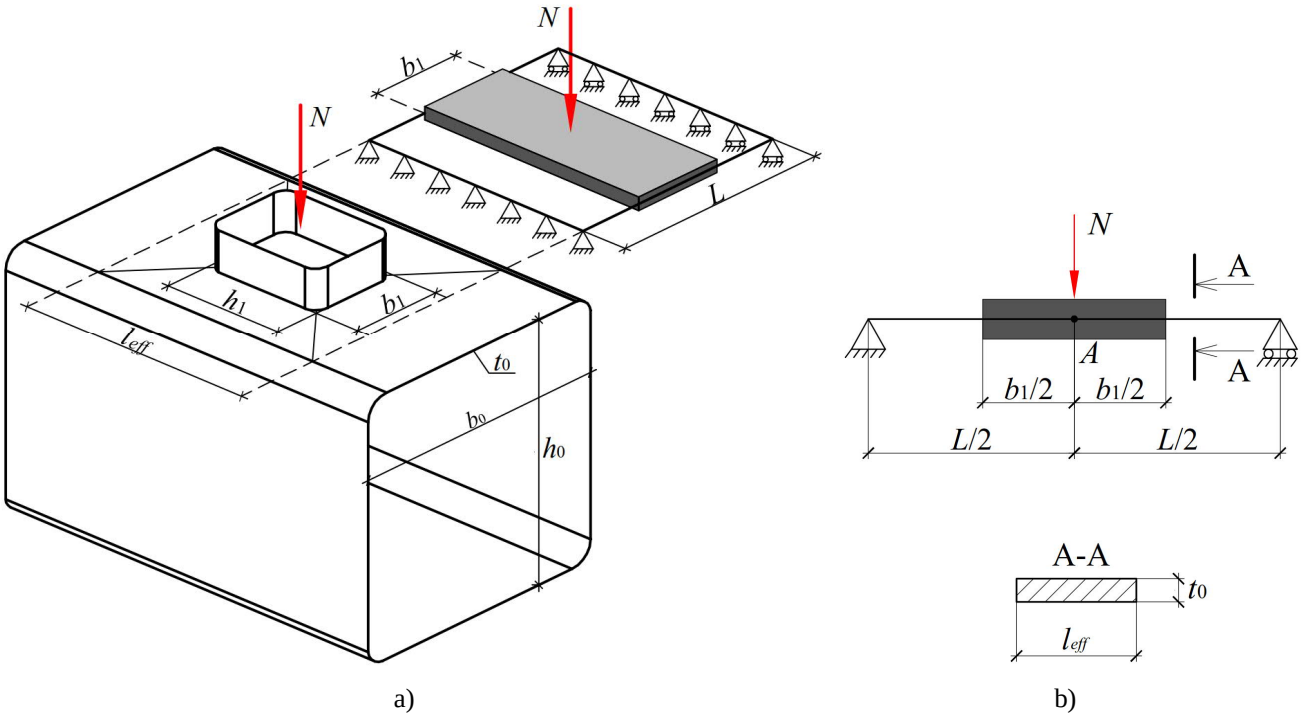

a) b)

Fig. 7. Component “chord face in bending”: a) spatial design model; b) 2D design model.

The stiffness of the component can be found as

$$k_a = \frac{N}{v(A)E} = \frac{4 l_{eff} t_0^3}{(L - b_1)^3} \tag{17}$$

The equivalent length l_{eff} remains the only unknown variable in Eq. (17). In this paper, it was determined numerically, employing the finite element (FE) software Abaqus/Standard [39]. To exclude a possible effect of the chord end conditions, the length of the chord was selected as $6b_0$ [40], while the brace length was chosen as b_1, as shown in Fig. 8a. According to [41], the model was constructed using quadratic solid finite elements with reduced integration (C3D20R), with two elements in the thickness direction. Since initial stiffness was the only requested outcome of the analyses, only elastic properties were introduced to the material model, with Young’s modulus of 210 GPa and Poisson’s ratio of 0.3. The brace was connected to the chord top face using a tie constraint. To avoid the contribution of the brace to the deformation of the joint, it was modelled with increased Young’s modulus of $210 \cdot 10^4$ GPa. The compressive axial load was applied using a single increment to point *O*, connected by a rigid body to the upper face of the brace. To avoid bending of the chord from the transverse force, it was restrained against vertical displacements along its length, as shown in Fig. 8a.

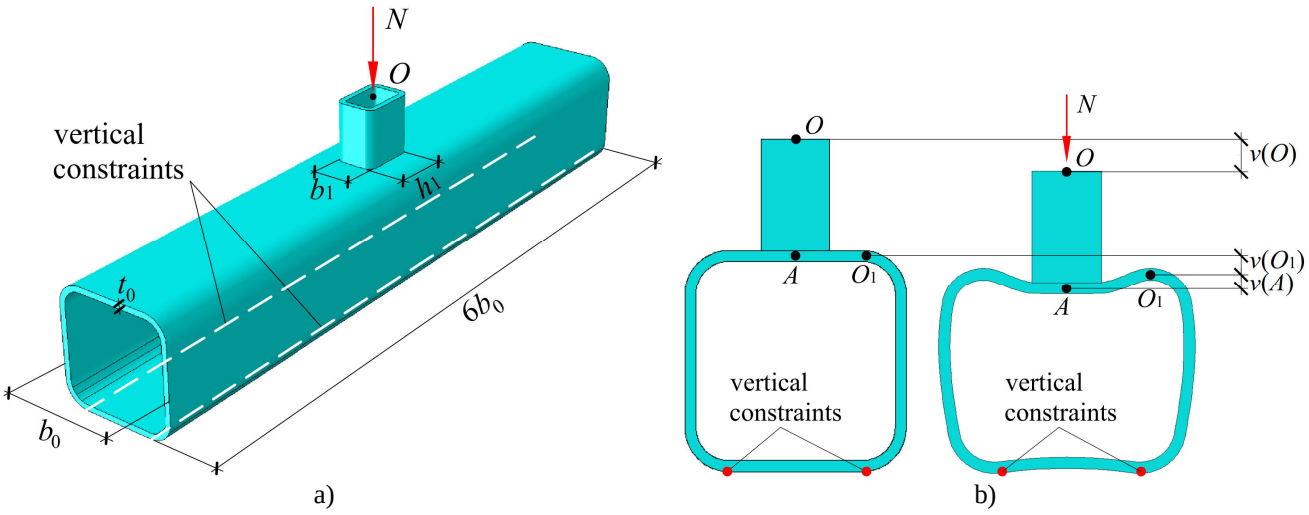

a) b)

Fig. 8. FE model: a) overall view; b) location of points with measured displacements.

Fig. 8b demonstrates two vertical displacements measured in the analyses: $v(O)$ corresponding to the displacement of the loading point O and $v(O_1)$ corresponding to the global displacement of the upper flange of the chord. The shortening of the brace was neglected due to its relatively high Young's modulus. The local displacement corresponding to the component "chord face in bending" was found as

$$v(A) = v(O) - v(O_1) \tag{18}$$

Following Eq. (16), the equivalent length l_{eff} was calculated as

$$l_{eff} = \frac{N(L - b_1)^3}{4Et_0^3 v(A)} \tag{19}$$

The equivalent length l_{eff} was determined for a series of joints with varying parameters b_0, b_1, h_1 and t_0. To avoid considering an extra variable h_0, only square hollow section were analyzed. For convenience, parameters b_1, h_1 and t_0 were correspondingly replaced by their relative ratios $\beta = b_1 / b_0$, $\alpha = h_1 / b_1$ and $2\gamma = b_0 / t_0$. EN 1993-1-8:2005 [5] provides the following limitations for these ratios: $0.25 \le \beta \le 1.0$, $0.5 \le \alpha \le 2.0$ and $10 \le 2\gamma \le 35$. Based on the numerical observations, for $\beta > 0.85$ the contribution of the component "chord face in bending" to the overall stiffness of the joint becomes negligibly small; therefore, the upper bound for β was reduced to 0.85. Table 5 provides the values for the considered variables.

Table 5. Values of variables used in FEM

Variable	Considered values
b_0 [mm]	100; 150; 200; 250; 300
$\beta = b_1 / b_0$	0.25; 0.40; 0.55; 0.70; 0.85
$2\gamma = b_0 / t_0$	10; 15; 20; 25; 30; 35
$\alpha = h_1 / b_1$	0.5; 1.0; 1.5; 2.0

Using Eq. (17), l_{eff} was calculated for varying joint parameters with $v(A)$ obtained by the finite element analysis. To analyze the behavior of l_{eff}, it was plotted against the introduced variables. As can be seen from Fig. 9, l_{eff} depends linearly on b_0 and α. According to Fig. 10, the dependence on β was assumed linear, while the influence of 2γ was found comparatively small and thus was ignored. To be consistent with the current terminology, α was replaced by the commonly used ratio $\eta = h_1 / b_0$. Finally, l_{eff} was approximated as

$$l_{eff} = h_1(2 - \beta) + 1.25 b_0 (1 - \beta)$$
$$\beta \le 0.85 \tag{20}$$

In relation to the numerical results, the proposed equation demonstrated sufficient accuracy, with $R^2 = 0.980$, $R^2_{adj} = 0.979$ and the average relative error of 4.1%. Since the component "chord face in bending" behaves similarly for T and X joints, the proposed equation can be also extended for X joints.

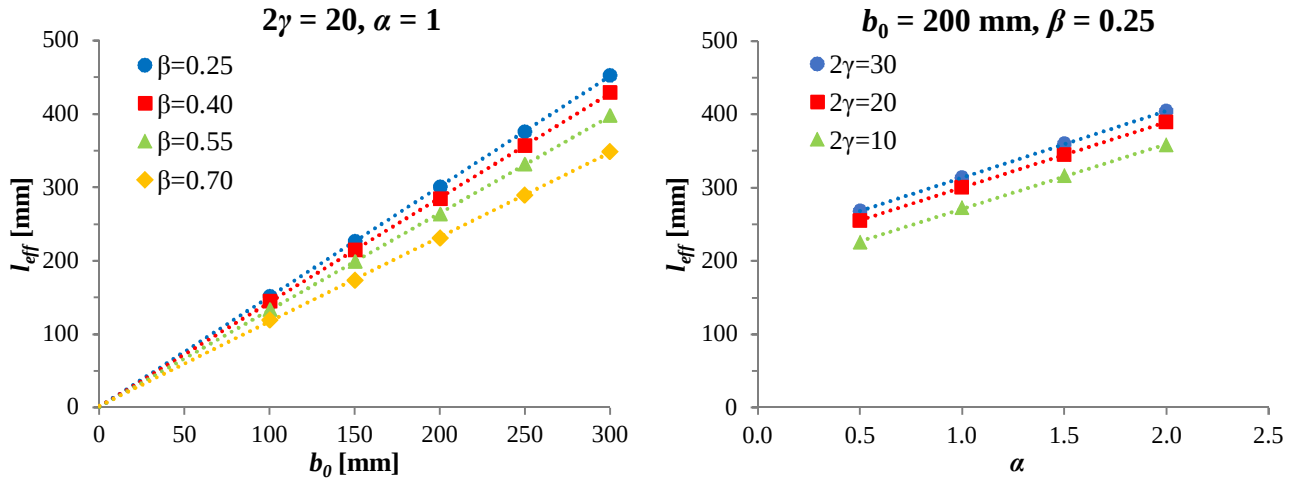

Fig. 9. Dependence of l_{eff} on b_0 and α.

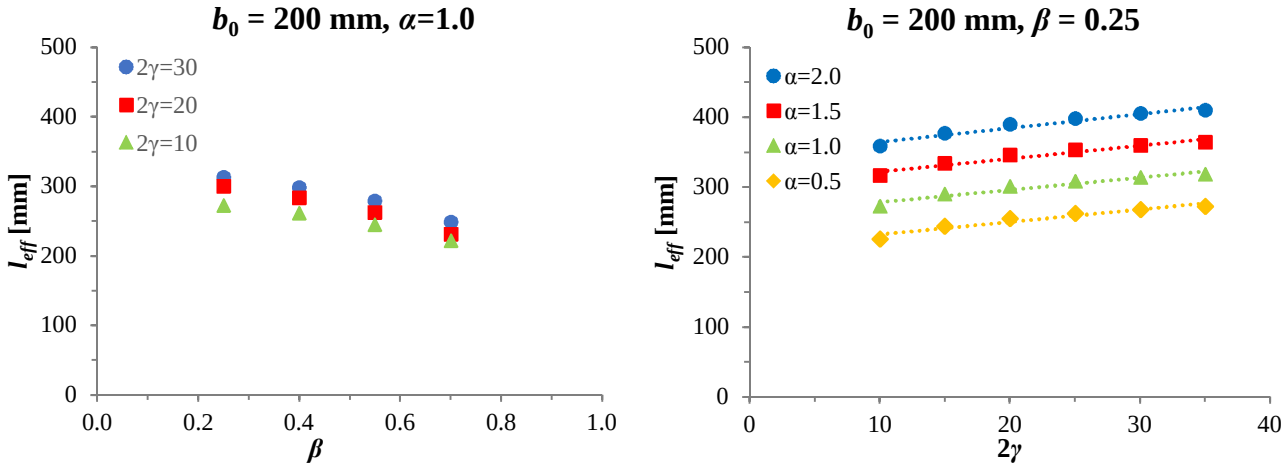

Fig. 10. Dependence of l_{eff} on β and 2γ.

4.2 Stiffness of the component "chord side walls in compression"

Consider an RHS T joint with a $b_0 \times h_0 \times t_0$ chord loaded axially by a $b_1 \times h_1$ brace with an axial force N. Fig. 11a shows the approximate deformation pattern for the compressed chord side wall. Considering it separately, the chord side wall can be replaced by a simply supported column of length $H = h_0 - t_0$ with an equivalent width b_{eff} and loaded by a compressive force $N/2$. It can be further simplified to a 2D beam model, shown in Fig. 11b.

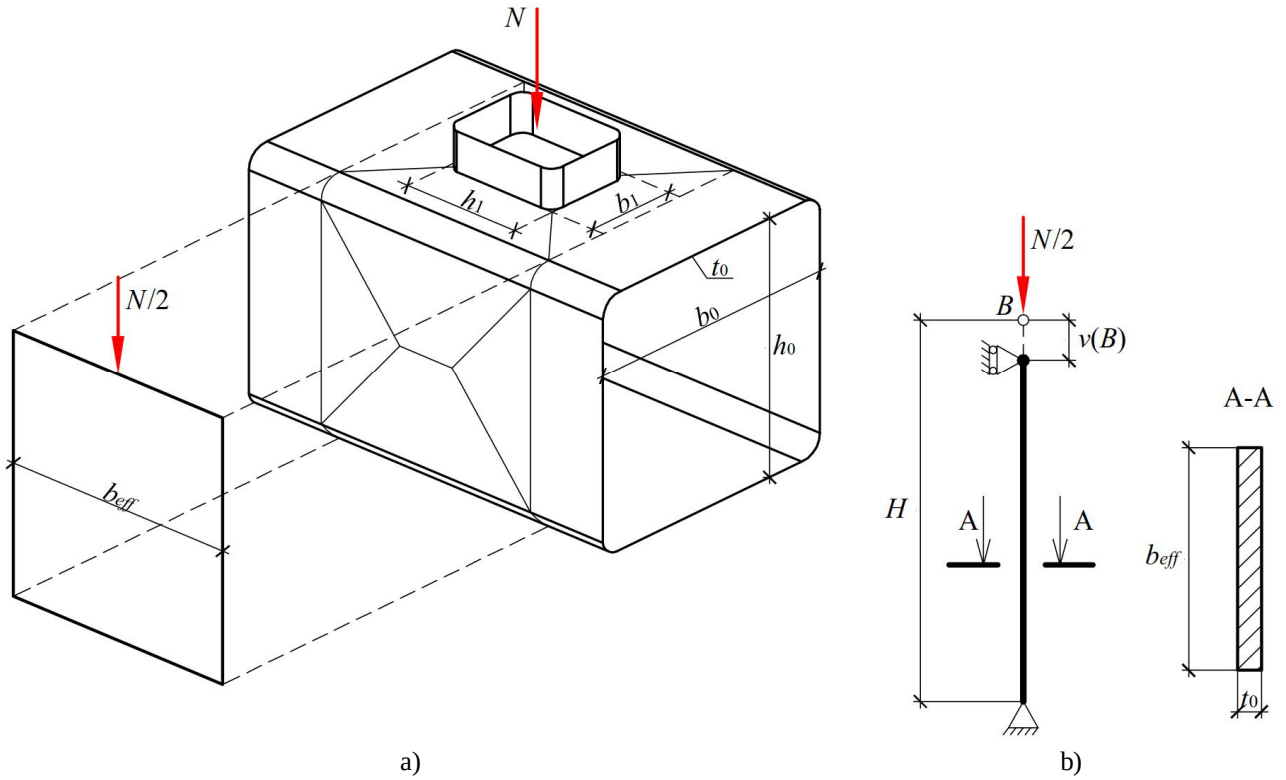

Fig. 11. Component "chord side walls in compression": a) spatial design model; b) 2D design model.

The vertical displacement at the end of the column (point B) can be found as

$$v(B) = \frac{0.5NH}{EA} = \frac{NH}{2Eb_{eff}t_0} \tag{21}$$

Then the stiffness of the component "chord side walls in compression" can be calculated as

$$k_b = \frac{N}{Ev(B)} = \frac{2b_{eff}t_0}{H} \tag{22}$$

This equation looks similar to Eq. (10) if b_{eff} and H are respectively replaced by $b_{eff,c,wc}$ and h_0. However, Eq. (22) does not take into account the coefficient 0.7, which is present in Eq. (10). The origin of this coefficient is difficult to trace. Probably, it represents a correction factor between the gradients for load introduction, as demonstrated by Grotmann & Sedlacek [11]:

$$r = \frac{\sqrt{3}}{2.5} = 0.693 \approx 0.7 \tag{23}$$

However, Grotmann & Sedlacek [11] employ a slightly different equation for the stiffness of this component and use this correction factor for the effective width b_{eff}. In this section, the equivalent width b_{eff} is determined by a series of numerical analyses, which by default consider this correction factor. This section employs the results of the FE analyses conducted for the component "chord face in bending". According to Fig. 8b, displacement $v(B)$ was found as equal to displacement $v(O_1)$. Moreover, additional analyses were conducted to consider joints with $\beta = 1.0$. These joints experienced no chord face bending; therefore, displacement $v(B)$ was calculated as equal to displacement $v(O)$. According to Eq. (22), the equivalent width b_{eff} was found as

$$b_{eff} = \frac{NH}{2Et_0 v(B)} \tag{24}$$

To analyze the behavior of b_{eff}, it was plotted against the introduced variables. The effective width b_{eff} was found to depend linearly on b_0 and α, as shown in Fig. 12. Similar to the component "chord face in bending", the influence of 2γ was found negligibly small and was ignored. At the same time, considerable nonlinear behavior was observed in relation to β, as shown in Fig. 13. To be consistent with the current terminology, α was replaced by the commonly used ratio $\eta = h_1 / b_0$. Finally, a curve fitting approach approximated b_{eff} as

$$b_{eff} = 0.025\left(h_1 (9\beta - 1) + \frac{2.4 b_0}{1.2 - \beta} \right) \tag{25}$$

In relation to the numerical results, the accuracy of the proposed equation was justified by $R^2 = 0.96$, $R^2_{adj} = 0.95$ and the average relative error of 11.2%. The component "chord side walls in buckling" governs the behavior of joints with $\beta > 0.85$. Table 1 demonstrated a clear difference between T and X joints with matching geometry. For this reason, the equations developed for this component cannot be extended for X joints and are limited only for T joints.

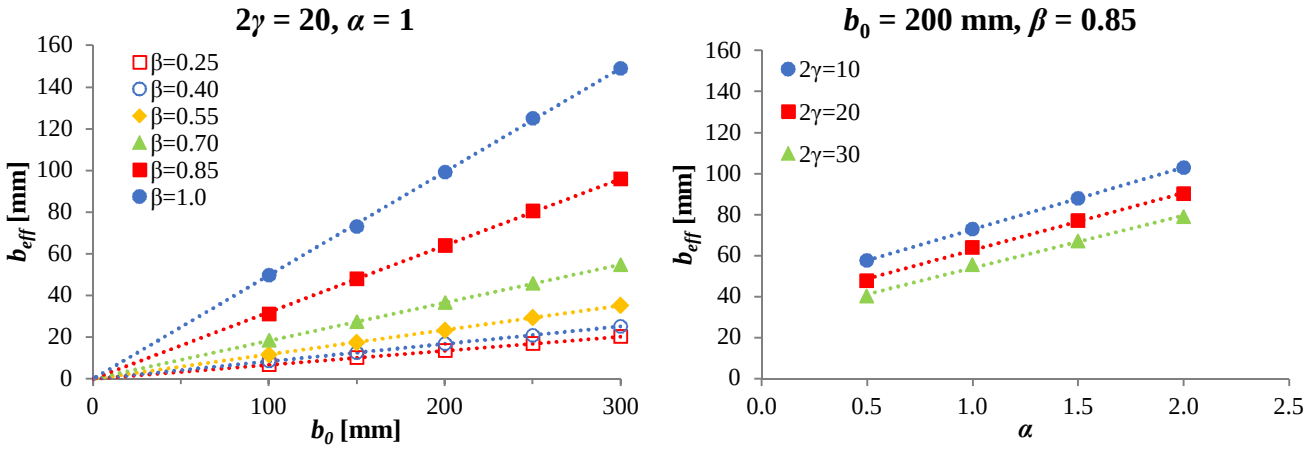

Fig. 12. Dependence of b_{eff} on b_0 and α.

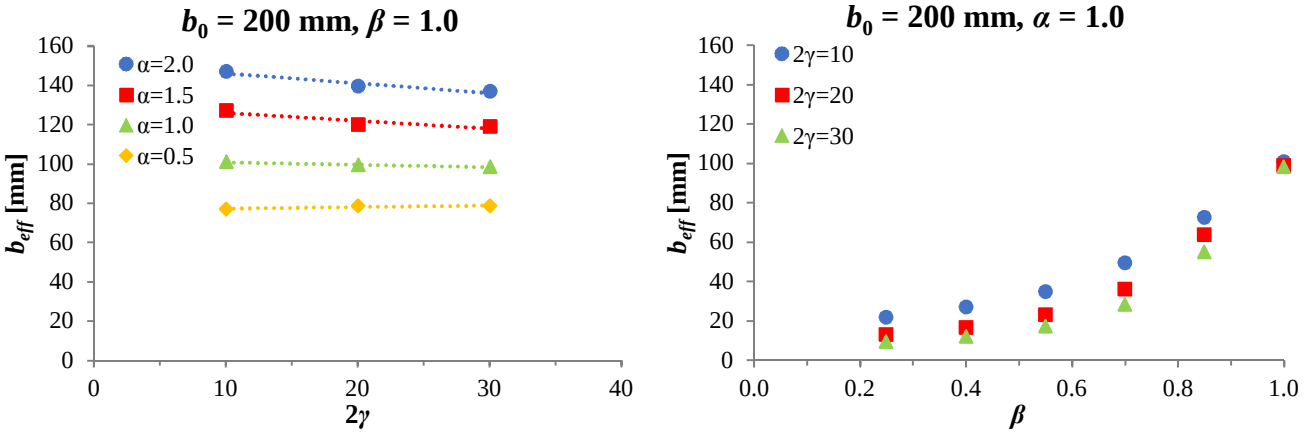

Fig. 13. Dependence of b_{eff} on 2γ and β.

4.3 Validation of the proposed equations

The developed equations were validated against the same experimental data as was used in Section 3. The stiffnesses of the components were calculated in accordance with the developed Eqs. (17) and (22), both neglecting (denoted as k_a and k_b) and considering the influence of fillet welds (denoted as $k_{a,eq}$ and $k_{b,eq}$). The corresponding theoretical stiffnesses are denoted as C and C_{eq}, respectively. Both were compared to experimental stiffness C_{exp}. The results of the validation are summarized in Table 6. For all the joints with $\beta \leq 0.85$, the theoretical prediction underestimates the experimental values, if fillet welds are ignored. If welds are taken into account, the prediction is more accurate and the C / C_{exp} ratio exceeds 1.0 in most cases, except joints T1 and T4. For these two joints, the exact throat thicknesses of welds were not provided by the authors and were determined as equal to $t_1/2$, as the minimum specified in the paper. If measured throat thicknesses were used instead, the ratio could have been closer to 1.0. The joints with $\beta = 1.0$ also demonstrate accurate prediction; however, any certain conclusions are complicated by the small amount of joints of available for the validation. It should be noted that for the joints with $\beta = 1.0$, the consideration of fillet welds does not bring any reasonable changes, since β cannot exceed 1.0. Generally, the results show that the developed equations provide sufficiently accurate prediction of initial axial stiffness and can be effectively used in the design of RHS T joints.

Table 6. Validation of the proposed theoretical approach

No.	Joint	β	β_{eq}	k_a [mm]	$k_{a,eq}$ [mm]	k_b [mm]	$k_{b,eq}$ [mm]	C [kN/mm]	C_{eq} [kN/mm]	C_{exp} [kN/mm]	C / C_{exp}	C_{eq} / C_{exp}
	$\beta \leq 0.85$											
3	S1B1C23	0.50	0.57	0.452	0.720	1.019	1.161	63	89	**74**	0.85	1.20
4	TN02N0	0.71	0.77	1.395	3.016	3.097	3.455	192	322	**280**	0.69	1.15
5	T1	0.50	0.53	0.349	0.419	1.513	1.604	60	70	**75**	0.79	0.93
6	T4	0.50	0.53	1.900	2.212	4.077	4.268	272	306	**400**	0.68	0.76
7	MPJT1	0.60	0.67	1.777	3.255	2.039	2.302	199	283	**230**	0.87	1.23
	Average										**0.77**	**1.06**
	Variance										**0.01**	**0.03**
	$\beta > 0.85$											
1	S1B1C11	1.00	1.00	-	-	2.445	2.445	489	489	**570**	0.86	0.86
2	S1B1C12	1.00	1.00	-	-	1.569	1.569	314	314	**330**	0.95	0.95
	Average										**0.90**	**0.90**
	Variance										**0.00**	**0.00**

Attention should be paid also to the approach that was employed to consider the influence of fillet welds. The results of the validation show that if welds are disregarded, initial stiffness in noticeably underestimated. The used solution allowed to compensate the observed underestimation for most of joints and obtain more accurate prediction of stiffness, although demonstrating excessive stiffness for joints 3 and 7. Unless a more accurate equation is developed based on extensive numerical and/or experimental values, this solution can be effectively employed as a rule of thumb for RHS T joints under axial loading. A similar approach was proposed for moment-loaded RHS joints in [37].

5. Chord stress function for initial axial stiffness

According to Wardenier [38], axial forces in the chord affect the structural behavior of RHS T joints. In particular, the reduction of resistance is determined by the so-called chord stress functions, the simplest of which is provided in EN 1993-1-8:2005 [5], Eq. (26). Some other functions for RHS T and X joints can be found in [42, 43].

$$k_n = \begin{cases} 1.3 - \dfrac{0.4|n|}{\beta} \le 1.0, & n > 0 \\ 1.0, & n < 0 \end{cases} \tag{26}$$

where n is the relative axial stress:

$$n = \frac{\sigma_0}{f_{y0}} = \frac{N_0}{A_0 f_{y0}} \tag{27}$$

where A_0 is the cross-sectional area of the chord and N_0 is the axial force in the chord. Although EN 1993-1-8:2005 [5] assumes negative n for tension and positive n for compression, most of publications [42–44] employ the inverse sign convention for n, which is also used in this paper.

In addition to resistance, a similar influence of chord axial stresses is also observed on the initial stiffness of tubular joints. Garifullin et al. [45] have shown that compressive normal stresses in the chord reduce the initial rotational stiffness of RHS T joints by 40%, while tensile stresses increase it by 30%. Such phenomenon might be particularly important for frame structures, where the stiffness of joints has to be considered in the global analysis. Such serious influence of chord axial stresses on initial stiffness can noticeably change the distribution of forces in the members of frames, affecting the results of the global analysis. This section numerically evaluates the effect of chord axial forces on the initial axial stiffness of RHS T joints and develops a corresponding chord stress function $k_{sn,N}$.

5.1 Numerical simulations

The analyses were conducted numerically, employing the same FE model as was used in Section 4. The scope of the study was restricted to square hollow sections to exclude the consideration of the additional variable b_0/h_0. All analyses were conducted for a joint with a 3.0 m long chord made of 300×300 mm cross-section. Following the requirements of EN 1993-1-8:2005 [5], the chord wall thickness t_0 varied from 8.5 mm (2γ = 35) to 30 mm (2γ = 10), whereas the brace width changed from 75 mm (β = 0.25) to 300 mm (β = 1.00), as shown in Table 7. The length of the brace was selected as equal to b_1. The brace wall thickness t_1 was determined so that it did not exceed the wall thickness of the chord t_0. The relative stress n in the chord was determined according to Eq. (27). All calculations employed the elastic-ideal plastic material model with E = 210 GPa and ν = 0.3. The analyses were conducted in two steps: after an axial load was applied to the chord on the first step, the end of the brace was loaded with a concentrated axial force N using only one increment to find the initial stiffness of the joint.

Table 7. Parameters of joints used in numerical simulations.

Chord		$300\times300\times t_0$			
	t_0 [mm]	8.5	10	20	30
	2γ	35	30	15	10
Brace		$b_1\times b_1\times t_1$			
	b_1 [mm]	75	180	255	300
	β	0.25	0.60	0.85	1.00
Steel grade	S355, S500, S700				
n	-0.95, -0.90, -0.80, -0.60, -0.30, 0, 0.30, 0.60, 0.80, 0.90, 0.95				

According to the obtained results, chord axial stresses significantly affected the initial axial stiffness of the joints. Figs. 14 and 16 plot the ratio C/C_0 for the joints with varying 2γ and β, where C is the stiffness with a relative axial stress n, C_0 is the stiffness with no axial stress. As can be seen, the observed effect has the similar pattern as in the case with initial rotational stiffness [45]. The maximum 35% reduction of stiffness is observed for compressive loads and 30% increase for tensile loads. The effect is particularly pronounced for the joints with small β and large 2γ. Moreover, the effect depends on the steel grade, increasing with the increase of yield strength, as shown in Fig. 15.

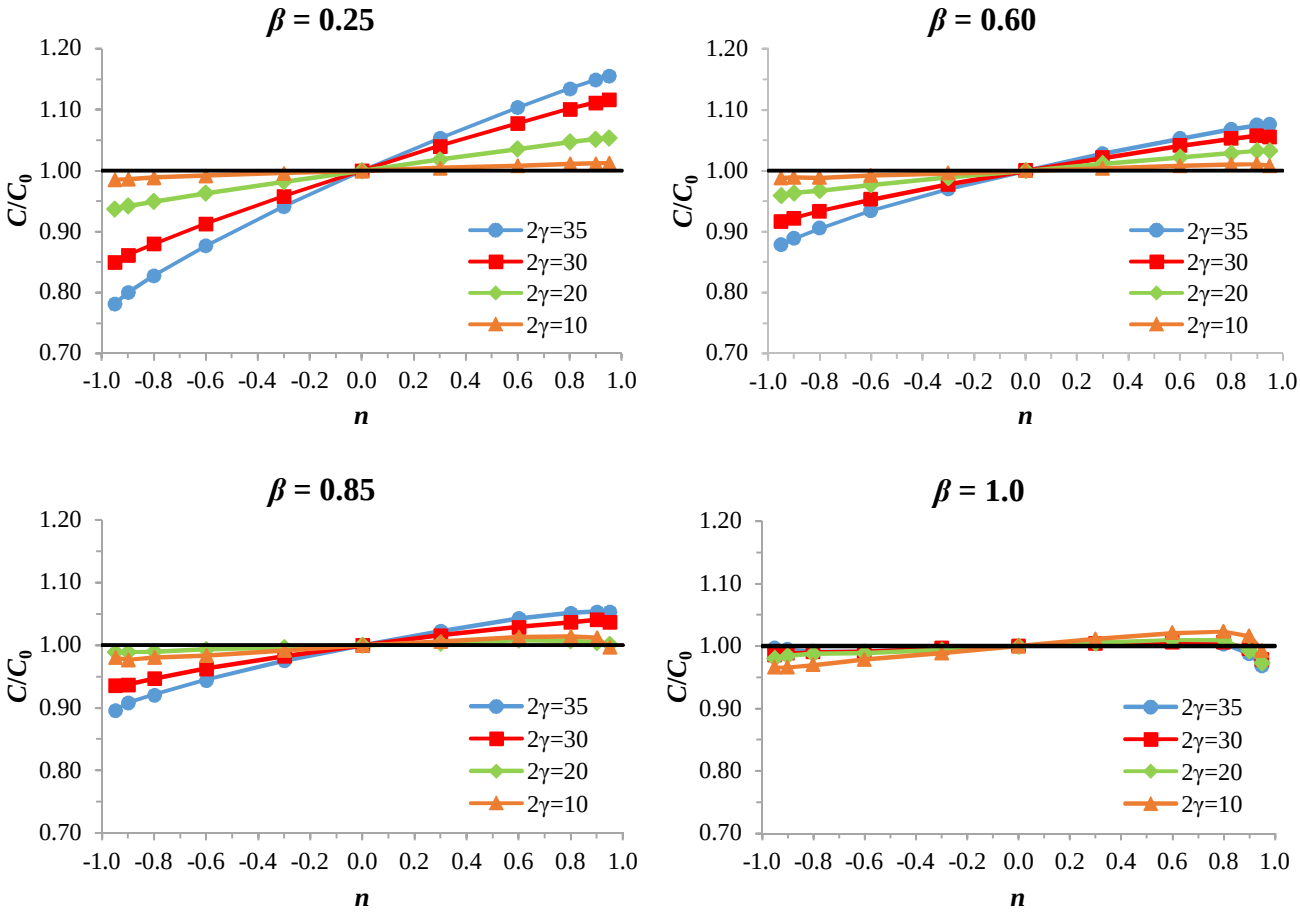

Fig. 14. Dependence of the effect on 2γ, S355.

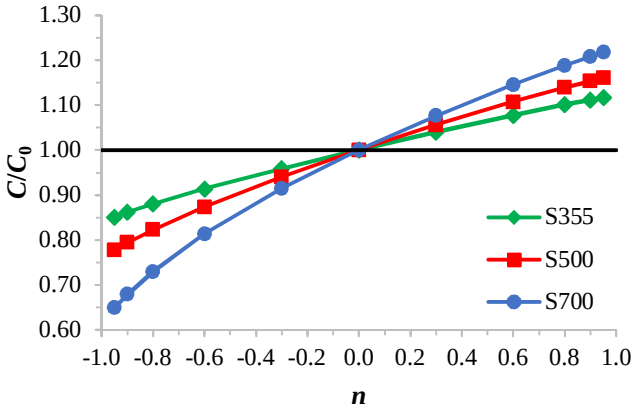

Fig. 15. Dependence of the effect on steel grade (2γ = 30, β = 0.25).

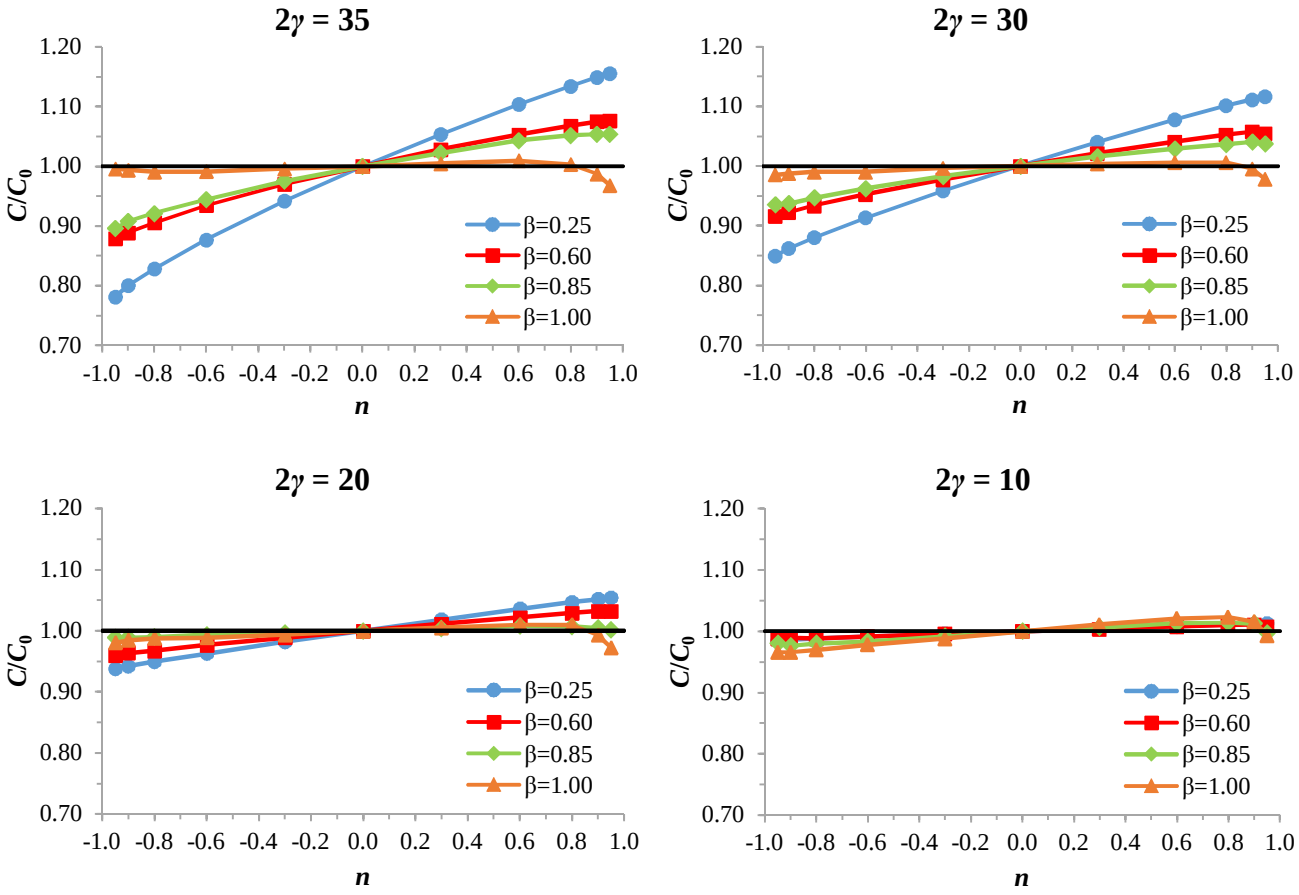

Fig. 16. Dependence of the effect on β, S355.

5.2 Chord stress function for initial axial stiffness

To take into account the influence of chord axial stresses, a corresponding chord stress function (CSF) was developed based on the obtained numerical results. Following the above observations, the function was found dependent on four variables: β, γ, f_{y0} (i.e., steel grade) and n. The assessment criteria included the coefficient of determination R^2, the adjusted coefficient of determination R^2_{adj}, the average percent error Δ_{av} and the maximum percent error Δ_{max}.

Table 8. Approximation based on the existing chord stress functions for the resistance.

Case	Equation	A	B	C	R^2	R^2_{adj}	Δ_{av} [%]	Δ_{max} [%]
1	$k_{sn,ip} = \begin{cases} 1.3 - \dfrac{0.4\lvert n\rvert}{\beta} \le 1.0, & n < 0 \\ 1.0, & n > 0 \end{cases}$	-	-	-	0.30	0.30	17.0	141.1
2	$k_{sn,ip} = 1 + A\dfrac{n}{\beta + B}, -0.99 \le n \le 0.99$	0.1	0.13	-	0.58	0.58	6.4	23.8
3	$k_{sn,ip} = \begin{cases} \left(1-\lvert n\rvert\right)^{0.6-0.5\beta}, & n < 0 \\ \left(1-\lvert n\rvert\right)^{0.1}, & n > 0 \end{cases}$	-	-	-	0.26	0.26	21.0	75.5
4	$k_{sn,ip} = \left(1+n\right)^{A+B\beta}$	0.45	0	-	0.47	0.47	29.9	73.7
5	$k_{sn,ip} = (1-n^2)^{0.8-0.8\beta+0.01\gamma}$	-	-	-	0.01	0.01	25.8	87.2
6	$k_{sn,ip} = (1-n^2)^{A+B\beta+C\gamma}$	0.1	0.1	0.1	0.01	0.01	53.1	99.0

Firstly, the paper tested the existing chord stress functions for resistance for their applicability to initial stiffness. The results are summarized in Table 8. Case 1 represents the current CSF in EN 1993-1-8:2005 [5], Eq. (26), providing very inaccurate results. Similar performance was observed for the functions proposed in [43], Case 3, and [42], Case 5. In addition, none of these functions considers the increase of

stiffness for tensile stresses. Cases 2, 4 and 6 represent the corresponding improvements of Cases 1, 3 and 5, originating from their general equations and adjusted using a curve fitting approach. As can be seen, none of the latter brings reasonable improvements in accuracy. These results demonstrated that the existing chord stress functions for resistance are inapplicable for initial stiffness.

A new CSF was developed based on the obtained numerical results. For some combinations of β and γ, the influence of chord axial forces is found to be negligibly small, as presented on Fig. 17a for S700 and $n = -0.95$. In the figure, the black dots represent the tested cases. In particular, the reduction of initial stiffness does not exceed 5% for the joints with small 2γ and large β; therefore, the introduction of a CSF seems unreasonable for these joints, particularly if its possible error exceeds 5%. For the remaining combinations of β and 2γ, the reduction is considerable, with the maximum value at the largest 2γ and smallest β. Following these observations, the analyzed area of joints was divided into two zones, as shown on Fig. 17b. The grey area corresponds to the joints for which no CSF is proposed, while the yellow zone denotes the area with the proposed CSF. The domain of CSF was specified with additional numerical analyses:

$$2\gamma \geq 12; \quad \beta \leq 0.9; \quad 40\beta - 2\gamma \leq 11 \tag{28}$$

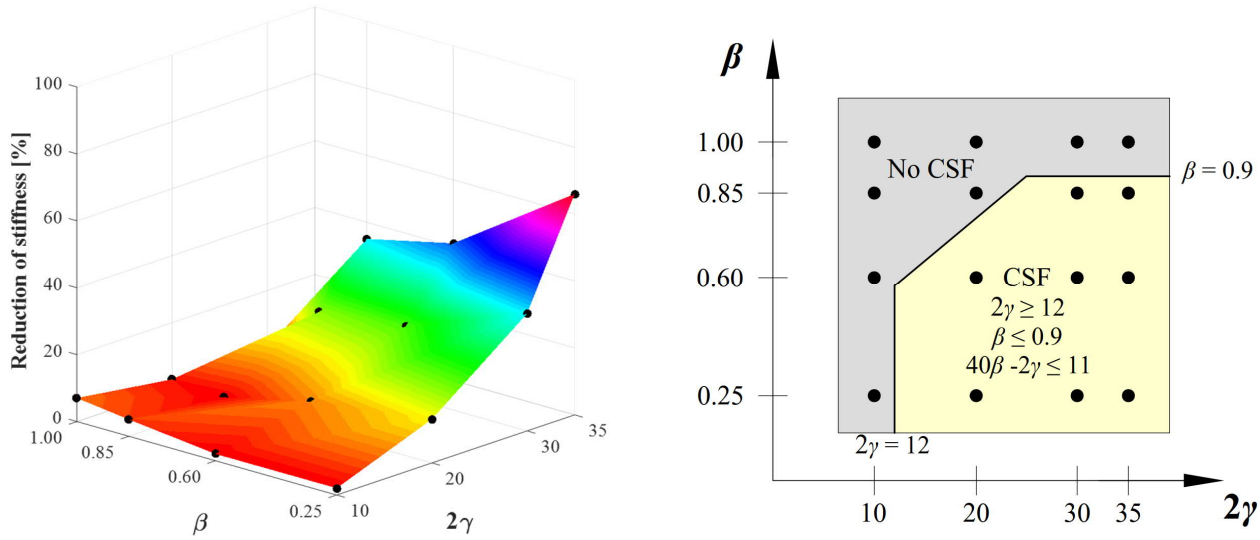

Fig. 17. a) Dependence on β and γ (S700, $n = -0.95$); b) domain of the proposed CSF.

According to Fig. 15, the proposed CSF was assumed to behave linearly for steel grades with 355 MPa $\leq f_{y0} \leq$ 500 MPa and nonlinearly for S700. For steel grades 500 MPa $< f_{y0} <$ 700 MPa, the values are proposed to be found by linear interpolation. The developed CSF is provided in Eq. (29).

$$\begin{aligned}
&\text{For } 355 \text{ MPa} \leq f_{y0} \leq 500 \text{ MPa}: \\
&k_{sn,N} = 1 + 10^{-5} f(\beta) f(\gamma) f\left(f_{y0}\right) n \\
&\text{For } 500 \text{ MPa} < f_{y0} < 700 \text{ MPa}: \\
&k_{sn,N} \text{ is the linear interpolation between S500 and S700} \\
&\text{For } f_{y0} = 700 \text{ MPa}: \\
&k_{sn,N} = 1 + 0.0008 f(\beta) f(\gamma)\left(n^3 - 1.25n^2 + 0.01 f\left(f_{y0}\right) n\right)
\end{aligned} \tag{29}$$

where

$$\begin{aligned}
f(\beta) &= -2\beta^2 + 1.6\beta + 0.3 \\
f(\gamma) &= 1.3\gamma^2 - 38 \\
f\left(f_{y0}\right) &= 0.02 f_{y0}^{1.4}
\end{aligned} \tag{30}$$

5.3 Validation of the proposed chord stress function

The validation of the proposed CSF was conducted with a series of independent FE results and employing the same FE model. To prove that the function is scalable in the chord width, the validation was conducted for the different chord size, 100×100 mm. The validation was performed for three chord wall thicknesses, two brace widths and two steel grades, as shown in Table 9. Although the grade S600 is not generally produced, it was used for scientific purposes, as an intermediate grade between S500 and S700. The brace wall thickness was selected so that it did not exceed that of the chord.

Table 9. Details of joints used for validation of CSF.

Chord, $b_0 \times h_0 \times t_0$	2γ	Brace, $b_1 \times h_1 \times t_1$	β	Steel grade
100×100×3	33.3	40×40×3	0.4	S420
100×100×4	25.0	80×80×3	0.8	S600
100×100×8	12.5			

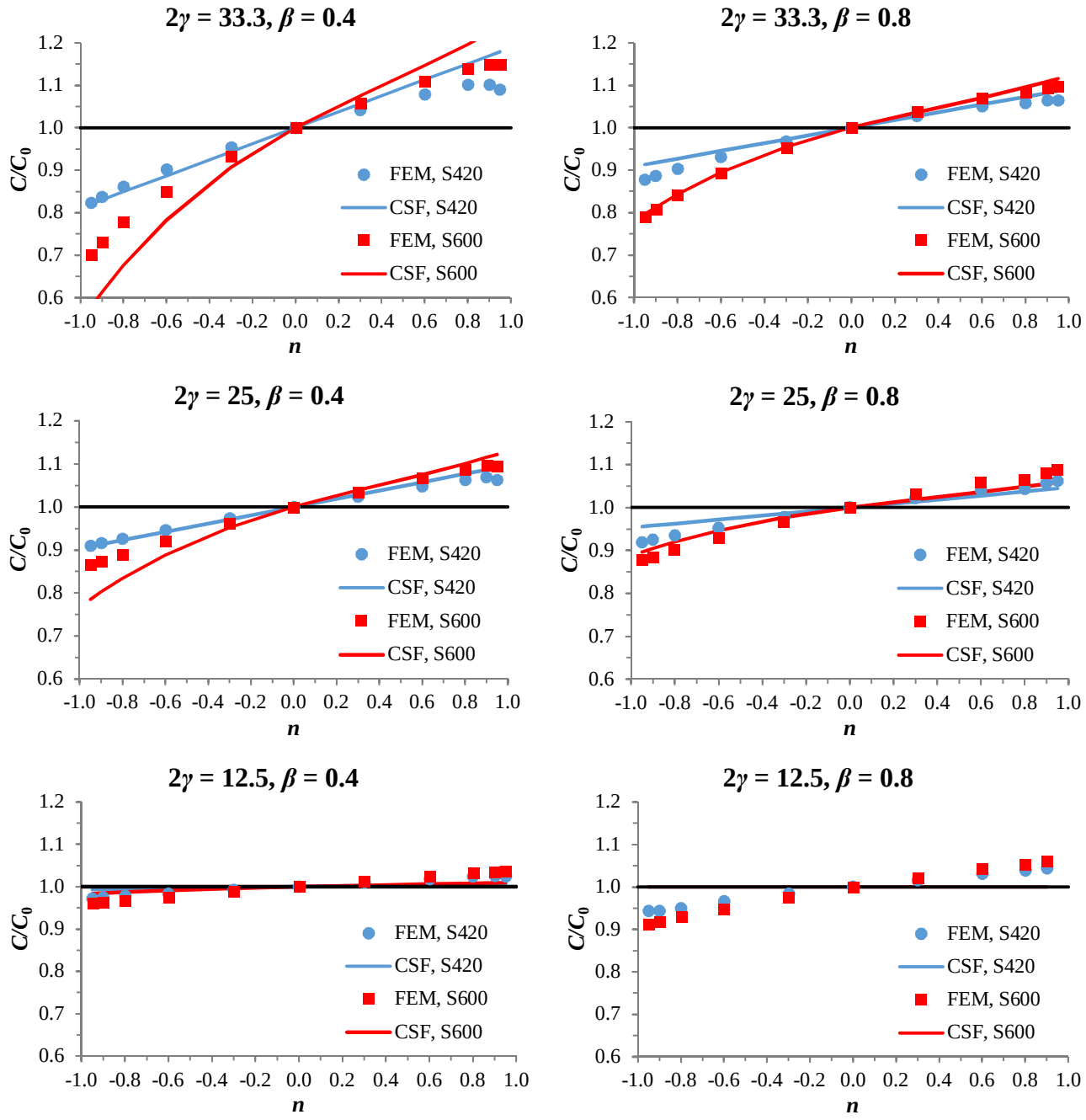

Fig. 18. Validation of the proposed CSF.

Fig. 18 presents the graphical validation of the developed chord stress function, plotting the ratio C/C_0 in relation to n, where C is the stiffness with a relative axial stress n, C_0 is the stiffness with no axial stress. As can be seen, the proposed CSF provides a sufficiently accurate prediction, with $R^2 = 0.94$, $R^2_{adj} = 0.93$, the average error is 2.3% and the maximum error is 17.3%. The case with $2\gamma = 12.5$ and $\beta = 0.8$ represents the only joint outside the domain of the CSF, meaning that no CSF is needed for it ($k_{sn,N} = 1.0$). The numerical simulations demonstrate 9% maximum reduction of initial stiffness for this joint, which is acceptable in practice. Taking the chord stress function into account, Eq. (1) can be modified as follows:

$$C_{j,ini,N} = \frac{k_{sn,N} E}{\sum_i \frac{1}{k_i}} \tag{31}$$

Conclusions

This paper considers the initial axial stiffness of tubular joints, employing the component method proposed by CIDECT. The paper considered the existing CIDECT approach for initial axial stiffness of RHS T joints and validated it against the existing experimental results. The validation has demonstrated that the existing equations for the stiffness of individual components lead to inaccurate results and cannot be reliable in the computational analysis. Moreover, in most cases, the stiffness equation for the component “chord face in bending” has violated its validity range. In addition, the direct comparison of the experimental stiffness of T and X joints with matching geometry have shown that X joints have considerably higher axial stiffness than T joints, therefore, they cannot be used to validate the theoretical approach for T joints.

Following the adopted component method, the paper has proposed new equations for the stiffness of the components “chord face in bending” and “chord side walls in compression”. The equations are based on simple mechanical modes, employing the concept of the effective length and width. Given that chord face bending develops similarly for T and X joints, a common equation has been proposed for the stiffness of the component “chord face in bending”. At the same time, the equation for the component “chord side walls in compression” has been limited only for T joints, given the abovementioned differences between the stiffness of T and X joints.

The developed equation were validated against the same experimental values. When the influence of fillet welds was disregarded, the prediction inconsiderably underestimated the stiffness of joints. The employed solution of de Matos et al. for fillet welds allowed to compensate the underestimation and obtain more accurate results, although overestimating the stiffness of some joints. In general, the proposed equations has demonstrated good correlation with the experimental results and can be recommended for the design of axially loaded RHS T joints.

It should be noted that the conducted research was considerably complicated by the small amount of the available experimental results. The second challenging issue was the determination of initial stiffness from the experimental data. In this paper, it was determined graphically based on the presented load-deformation curves. This approach is rather complicated and might lead to inaccurate results. Such researches, where theoretical solutions are evaluated with existing experimental data, can be conducted more effectively if in addition to resistance and load-deformation curves, authors also provide the exact values of initial stiffness.

The second part of the paper investigated the influence of chord axial stresses on the initial axial stiffness of RHS T joints. The conducted numerical simulations demonstrated that compressive stresses reduce stiffness by 35%, while tensile stresses increase it by 30%. The effect was found dependent on the geometry and the steel grade of joints, being particularly strong for joints with high 2γ, small β and high steel grades. To take this influence into account, the paper has developed a corresponding chord stress function. The validation with a series of independent numerical data has shown the sufficient accuracy of the proposed function, which can be further verified against new experimental results.

References

[1] H. Boel, *Buckling length factors of hollow section members in lattice girders*. Master Thesis. Eindhoven: Eindhoven University of Technology, 2010.

[2] H.H. Snijder, H.D. Boel, J.C.D. Hoenderkamp, R.C. Spoorenberg, Buckling length factors for welded lattice girders with hollow section braces and chords, Proceedings of the 6th European Conference on Steel and Composite Structures (Eurosteel 2011), 31 August - 2 September 2011, Budapest, Hungary, 2011, pp. 1881–1886.

[3] Ä. Haakana, *In-plane buckling and semi-rigid joints of tubular high strength steel trusses*. Master of Science Thesis. Tampere: Tampere University of Technology, 2014.

[4] M. Garifullin, S. Pajunen, K. Mela, M. Heinisuo, 3D component method for welded tubular T joints, Tubular Structures XVI: Proceedings of the 16th International Symposium for Tubular Structures (ISTS 2017, 4-6 December 2017, Melbourne, Australia), 2018, pp. 165–173.

[5] CEN, *Eurocode 3: Design of steel structures – Part 1-8: Design of joints (EN 1993-1-8:2005)*. Brussels, 2005.

[6] J.A. Packer, J. Wardenier, X.-L. Zhao, G.J. van der Vegte, Y. Kurobane, *Design guide for rectangular hollow section (RHS) joints under predominantly static loading. CIDECT Design Guide No. 3.*, 2nd ed. LSS Verlag, 2009.

[7] Y. Yu, *The static strength of uniplanar and multiplanar connections in rectangular hollow sections*. PhD thesis. Delft: Delft University of Technology, 1997.

[8] J.J. Cao, J.A. Packer, G.J. Yang, Yield line analysis of RHS connections with axial loads, J. Constr. Steel Res. 48(1) (1998) 1–25.

[9] X.-L. Zhao, J. Wardenier, J.A. Packer, G.J. van der Vegte, Current static design guidance for hollow-section joints, Proc. Inst. Civ. Eng. — Struct. Build. 163(6) (2010) 361–373.

[10] P. Mäkeläinen, R. Puthli, F. Bijlaard, Strength, stiffness and nonlinear behaviour of simple tubular joints, IABSE Congr. Rep. 13 (1988) 635–640.

[11] D. Grotmann, G. Sedlacek, *Rotational stiffness of welded RHS beam-to-column joints. Cidect 5BB-8/98*. Aachen: RWTH-Aachen, 1998.

[12] R.M.M.P. de Matos, L.F. Costa-Neves, L.R.O. de Lima, P.C.G.S. Vellasco, J.G.S. da Silva, Resistance and elastic stiffness of RHS “T” joints: Part I – Axial brace loading, Lat. Am. J. Solids Struct. 12(11) (2015) 2159–2179.

[13] L.F. Costa-Neves, *Monotonic and cyclic behaviour of minor-axis and hollow section joints in steel and composite structures. Doctoral Thesis*. University of Coimbra, 2014.

[14] K. Weynand, J.-P. Jaspart, J.-F. Demonceau, L. Zhang, *Component method for tubular joints*. CIDECT Report 16F – 3/15, 2015.

[15] P. Zoetemeijer, Design method for the tension side of statically loaded, bolted beam-to-column connections, Heron. 20(1) (1974) 1–59.

[16] F. Tschemmernegg, A. Tautschnig, H. Klein, C. Braun, C. Humer, Zur Nachgiebigkeit von Rahmenknoten – Teil 1, Stahlbau. 56(10) (1987) 299–306 (in German).

[17] F. Wald, *Column bases*. Prague: CTU Prague, 1995.

[18] L. Leston-Jones, *The influence of semi-rigid connections on the performance of steel framed structures in fire*. PhD Thesis. University of Sheffield, 1997.

[19] A.M. Girão Coelho, F.S.K. Bijlaard, Experimental behaviour of high strength steel end-plate connections, J. Constr. Steel Res. 63(9) (2007) 1228–1240.

[20] L.S. da Silva, Towards a consistent design approach for steel joints under generalized loading, J. Constr. Steel Res. 64(9) (2008) 1059–1075.

[21] M. Heinisuo, H. Ronni, H. Perttola, A. Aalto, T. Tiainen, End and base plate joints with corner bolts for rectangular tubular member, J. Constr. Steel Res. 75 (2012) 85–92.

[22] K. Weynand, J.-P. Jaspart, Extension of the component method to joints in tubular construction, Tubular Structures IX: Proceedings of the Ninth International Symposium and Euroconference, Dusseldorf, Germany, 3-5 April 2001, 2001, pp. 517–524.

[23] J.-P. Jaspart, C. Pietrapertosa, K. Weynand, E. Busse, R. Klinkhammer, *Development of a full consistent design approach for bolted and welded joints in building frames and trusses between steel members made of hollow and / or open sections – Application of the component method.*

Volume 1 – Practical guidelines. CIDECT Report: 5BP-4/05, 2005.
[24] M. Garifullin, M. Bronzova, T. Jokinen, M. Heinisuo, B. Kovačič, Effect of fillet welds on initial rotational stiffness of welded tubular joints, Procedia Eng. 165 (2016) 1643–1650.
[25] C. Málaga-Chuquitaype, A.Y. Elghazouli, Component-based mechanical models for blind-bolted angle connections, Eng. Struct. 32(10) (2010) 3048–3067.
[26] J.-P. Jaspart, *Etude de la semi-rigidité des noeuds pouter-colonne et son influence sur la résistance et la stabilité des ossatures en acier*. Doctor of Science thesis. University of Liège (in French), 1991.
[27] C. López-Colina, M.A. Serrano-López, F.L. Gayarre, J.J. Del Coz-Díaz, Stiffness of the component "lateral faces of RHS" at high temperature, J. Constr. Steel Res. 67(12) (2011) 1835–1842.
[28] B. Kato, I. Nishiyama, T-joints made of rectangular tubes, International Specialty Conference on Cold-Formed Steel Structures. 3, 1980, pp. 663–679.
[29] X.-L. Zhao, G.J. Hancock, T-joints in rectangular hollow sections subject to combined actions, J. Struct. Eng. 117(8) (1991) 2258–2277.
[30] G. Davies, P. Crockett, The strength of welded T-DT joints in rectangular and circular hollow section under variable axial loads, J. Constr. Steel Res. 37(1) (1996) 1–31.
[31] A. Nizer, L.R.O. de Lima, P.C.G.S. Vellasco, S.A.L. de Andrade, E. da S. Goulart, A.T. da Silva, L.F. Costa-Neves, Experimental and numerical assessment of RHS T-joints subjected to brace and chord axial forces, Steel Constr. 9(4) (2016) 315–322.
[32] J. Becque, T. Wilkinson, The capacity of grade C450 cold-formed rectangular hollow section T and X connections: An experimental investigation, J. Constr. Steel Res. 133 (2017) 345–359.
[33] M. Pandey, B. Young, High strength steel tubular X-joints — an experimental insight under axial compression, Tubular Structures XVI: Proceedings of the 16th International Symposium for Tubular Structures (ISTS 2017, 4-6 December 2017, Melbourne, Australia), 2018, pp. 223–230.
[34] K.J.R. Rasmussen, B. Young, Tests of X- and K-joints in SHS stainless steel tubes, J. Struct. Eng. 127(10) (2001) 1173–1182.
[35] R. Feng, B. Young, Experimental investigation of cold-formed stainless steel tubular T-joints, Thin-Walled Struct. 46(10) (2008) 1129–1142.
[36] R. Feng, B. Young, Tests and behaviour of cold-formed stainless steel tubular X-joints, Thin-Walled Struct. 48(12) (2010) 921–934.
[37] M. Heinisuo, M. Garifullin, T. Jokinen, T. Tiainen, K. Mela, Surrogate modeling for rotational stiffness of welded tubular Y-joints, Connections in Steel Structures VIII, 2016, pp. 285–294.
[38] J. Wardenier, *Hollow section joints*. Delft: Delft University of Technology, 1982.
[39] Abaqus, *Abaqus 6.12. Getting Started with Abaqus: Interactive Edition*. Dassault Systèmes, 695 p., 2012.
[40] G.J. van der Vegte, Y. Makino, Further research on chord length and boundary conditions of CHS T- and X-joints, Adv. Steel Constr. 6(3) (2010) 879–890.
[41] G.J. van der Vegte, J. Wardenier, R.S. Puthli, FE analysis for welded hollow-section joints and bolted joints, Proc. Inst. Civ. Eng. — Struct. Build. 163(SB6) (2010) 427–437.
[42] D.K. Liu, J. Wardenier, G.J. van der Vegte, New chord stress functions for rectangular hollow section joints, The Fourteenth International Offshore and Polar Engineering Conference, 2004, pp. 178–185.
[43] J. Wardenier, G.J. van der Vegte, D.K. Liu, Chord stress function for rectangular hollow section X and T joints, Proceedings of the Seventeenth International Offshore and Polar Engineering Conference, 2007, pp. 3363–3370.
[44] A. Lipp, T. Ummenhofer, Influence of tensile chord stresses on the strength of CHS X-joints – Experimental and numerical investigations, Tubular Structures XV: Proceedings of the 15th International Symposium on Tubular Structures, Rio de Janeiro, Brazil, 27-29 May 2015, 2015, pp. 379–386.
[45] M. Garifullin, S. Pajunen, K. Mela, M. Heinisuo, J. Havula, Initial in-plane rotational stiffness of welded RHS T joints with axial force in main member, J. Constr. Steel Res. 139 (2017) 353–362.